EARTHQUAKE-INDUCED BUILDING DAMAGE ESTIMATION USING ALOS/PALSAR OBSERVING THE 2007 PERU EARTHQUAKE

Masashi MATSUOKA[a] and Miguel ESTRADA[b]

[a] Associate Professor, Dept. of Built Environment, Tokyo Institute of Technology,
4259-G3-2 Nagatsuta, Midori-ku, Yokohama 226-8502, Japan;
Tel: +81(0) 45-924-5605; Fax. +81(0) 45-924-5574
E-mail: matsuoka.m.ab@m.titech.ac.jp
[b] Associate Professor, Japan-Peru Center for Earthquake Engineering and Disaster Mitigation (CISMID),
National University of Engineering, Av. Túpac Amaru 1150, Lima 25, Peru;
Tel: +51(0) 1-4820790; Fax. +51(0) 1-4820790
E-mail: estrada@uni.edu.pe

KEY WORDS: severe damage ratio, ALOS/PALSAR, the 2007 Peru earthquake, likelihood function, backscattering coefficient

Abstract: With the aim of developing a model for estimating building damage from synthetic aperture radar (SAR) data at L-band, which is appropriate for Peru, we propose a regression discriminant function based on field survey data in Pisco, which was seriously affected by the 2007 Peru earthquake. The function can discriminate damage ranks corresponding to the severe damage ratio of buildings using ALOS/PALSAR imagery of the disaster area before and after the earthquake. By calculating the differences in and correlations of backscattering coefficients, which were explanatory variables of the regression discriminant function, we determined an optimum window size capable of estimating the degree of damage more accurately. A normalized likelihood function for the severe damage ratio was developed based on discriminant scores of the regression discriminant function.

INTRODUCTION

Satellite remote sensing is being increasingly used for quick assessment of the impact of natural disasters occurring frequently all over the world (International Charter Space and Major Disaster, 2012). A synthetic aperture radar (SAR), a type of remote sensing sensor, can observe the surface of the earth in the daytime and nighttime, regardless of weather. If visual interpretation of damage from SAR imagery is practicable, it will complement the visual interpretation from optical sensor imagery. However, unlike optical sensor images, which look like photographs, SAR imagery is a representation of the intensity of backscattering of microwaves from the ground surface and is unfamiliar to nonexperts. It is therefore difficult to visually interpret damage from SAR images by volunteer-based many interpreters, namely, crowdsourcing (Ghosh et al., 2011). It is thus expected that extraction of damage from SAR imagery will be done by computer-based image processing (Arciniegas et al., 2007; Midorikawa and Miura, 2010). Therefore, estimation models for building damage ratios were proposed (Ito and Hosokawa, 2002; Matsuoka and Yamazaki, 2004; Nojima et al., 2006). They were based on C-band (wavelength: approximately 5.7 cm) SAR imagery in which building damage data obtained from detailed field surveys conducted after the Kobe earthquake in 1995 were used as ground-truth data, and applicability of one of the models used for damage extraction in other earthquakes occurring in various countries and regions was investigated (Matsuoka and Yamazaki, 2010). Furthermore, the model was improved so that it was also applicable to imagery obtained by JERS-1/SAR and ALOS/PALSAR (hereafter referred to as PALSAR imagery), which are L-band (wavelength: approximately 23 cm) SAR mounted on Japanese satellites. It was then applied to PALSAR imagery obtained at the 2007 Peru earthquake and the 2008 Wenchuan, China earthquake (Matsuoka and Nojima, 2010). It was found from comparison with damage assessment reports of these earthquakes, etc., local damage areas could not be detected because the model was based on the ground-truth data of the 1995 Kobe earthquake. In other words, it was demonstrated that application of the model to other countries and regions, which have different urban structures, building types, and damage situations from Japan, gave inaccurate results (Matsuoka and Nojima, 2010).

Following procedures reported in our previous papers (Nojima et al., 2006; Matsuoka and Nojima, 2010), this paper aims to develop a model for estimating the severe damage ratio of buildings that reflects the building types and damage situation in Peru. It can be said that the model is an estimation model for severe damage ratio optimized for Peru, because it is based on PALSAR imagery of Pisco at the 2007 Peru earthquake and on the building damage data obtained from field surveys. To be more specific, an optimum window size for image processing was determined and a normalized likelihood function for the severe damage ratio was derived.

PALSAR IMAGES AND FIELD SURVEY DATA

Indices obtained from PALSAR imagery and image processing

On August 15, 2007, the Peru earthquake measuring M8.0 occurred, the epicenter of which was 40-km northwest of Chincha. The city of Pisco in the Ica Region and the surrounding area were devastated by the earthquake; more than 500 people died or were missing and more than 35,000 buildings were completely destroyed. About 2 weeks after the earthquake, PALSAR imagery of the coastal area with high resolution was obtained. Figure 1 (a) and (b) shows images obtained before and after the earthquake (before: July 12, 2007; after: August 27, 2007). The nominal ground resolution was approximately 10 m and the pixel size of images was 12.5 m.

Two indices, differences (between post- and pre- earthquake images) and correlation coefficients of backscattering coefficients, were calculated from the pre- and post-earthquake PALSAR images. Following accurate positioning of both the post- and pre-event images, a speckle reduction filter is applied to each image (Lee, 1980). Then, differences and correlation coefficients are calculated from the following equations (1) and (2). The difference is obtained by subtracting the average value of the backscattering coefficient within an $N \times N$ pixel window of the pre-event image from that of the post-event image. The correlation coefficient is also calculated from the same $N \times N$ pixel window. The analysis result from the Kobe earthquake showed that differences (after – before) yielded negative values, with the spatial distribution of backscattering coefficients decreasing with building damage and as compared with that in pre-event, resulting in an overall decrease in correlation coefficient (Matsuoka and Yamazaki, 2004).

$$d = 10 \cdot \log_{10} \bar{I}a_i - 10 \cdot \log_{10} \bar{I}b_i \tag{1}$$

$$r = \frac{N\sum_{i=1}^{N} Ia_i Ib_i - \sum_{i=1}^{N} Ia_i \sum_{i=1}^{N} Ib_i}{\sqrt{\left(N\sum_{i=1}^{N} Ia_i^2 - \left(\sum_{i=1}^{N} Ia_i\right)^2\right) \cdot \left(N\sum_{i=1}^{N} Ib_i^2 - \left(\sum_{i=1}^{N} Ib_i\right)^2\right)}} \tag{2}$$

where d represents the difference in backscattering coefficients [dB], r is the correlation coefficient, and N is the number of pixels within a window to be calculated. Ia_i and Ib_i represent the i-th pixel values of the post- and pre-event images, respectively, and $\bar{I}a_i$ and $\bar{I}b_i$ represent the average values of $N \times N$ pixels surrounding the i-th pixel.

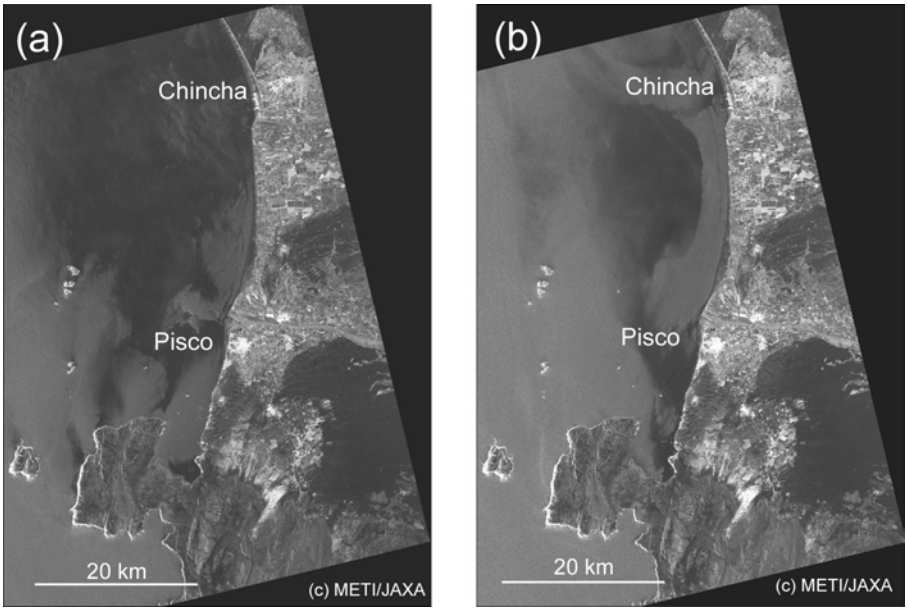

Figure 1: PALSAR imagery obtained before and after the 2007 Peru earthquake: (a) July 12, 2007; (b) August 27, 2007.

Severe damage ratio of buildings based on the field survey data

The target area of the damage estimation model is the city of Pisco. Damage data used in this study were collected by members of the Japan-Peru Center for Earthquake Engineering and Disaster Mitigation (CISMID), National University of Engineering, Peru, who performed on-site investigation of buildings in more than 10,000 lots in detail just after the earthquake (Estrada et al., 2008) and were considered to be the most reliable data on the Peru earthquake. Investigation items included building lot codes, building use, structure types, floor number, and damage level, all of which were combined with geographic information system (GIS) data. Approximately 97% of buildings in the area were masonry structures (about 18% of which were adobe structures and about 79% of which were burnt brick structures), which have low toughness and are prone to collapse in general. In the earthquake, adobe structure buildings were greatly damaged. A lot and a building were mostly in a one-to-one correspondence; when multiple buildings were located in a large lot, information on the most damaged building was recorded. Figure 2 (a) shows the distribution of damage level by lot based on the field survey in Pisco.

Damage level was classified into the following four levels: Grave (Serious), Severo (Severe), Leve (Slight), and Sin daño (No-damage); lots that could not be investigated were represented as "Not available." Grave corresponds to G5 in the classification of the European Macroseismic Scale (EMS-98) (Grünthal, 1998), Severo to G4 and G3, Leve to G2, and Sin daño to G1. Based on these GIS data, the damage ratio was calculated. In order to take size of lots and vacant lots into consideration and to calculate reliable damage ratio, the city of Pisco was split into a grid of 3.75 × 3.75 arc-seconds (approximately 120-m mesh) and estimation was performed only on grids with 10 or more lots. The severe damage ratio of buildings in a grid was calculated as the ratio of the number of Grave to the total number of buildings in the grid. The severe damage ratio was classified into the following six damage ranks: C1, 0% severe damage ratio in a grid; C2, more than 0% and less than 6.25%; C3, 6.25% or more and less than 12.5%; C4, 12.5% or more and less than 25%; C5, 25% or more and less than 50%; and C6, 50% or more. Table 1 shows the correspondence between the damage rank, the severe damage ratio and the median values. The distribution of the severe damage ratio is shown in Figure 2 (b).

Table 1: Range of the severe damage ratio and the median values for each damage rank

Damage Rank	Severe Damage Ratio D (%)	Median Value (%)
C1	$D = 0$	0.0
C2	$0 < D < 6.25$	3.13
C3	$6.25 \leq D < 12.5$	9.38
C4	$12.5 \leq D < 25$	18.75
C5	$25 \leq D < 50$	37.5
C6	$50 \leq D \leq 100$	75.0

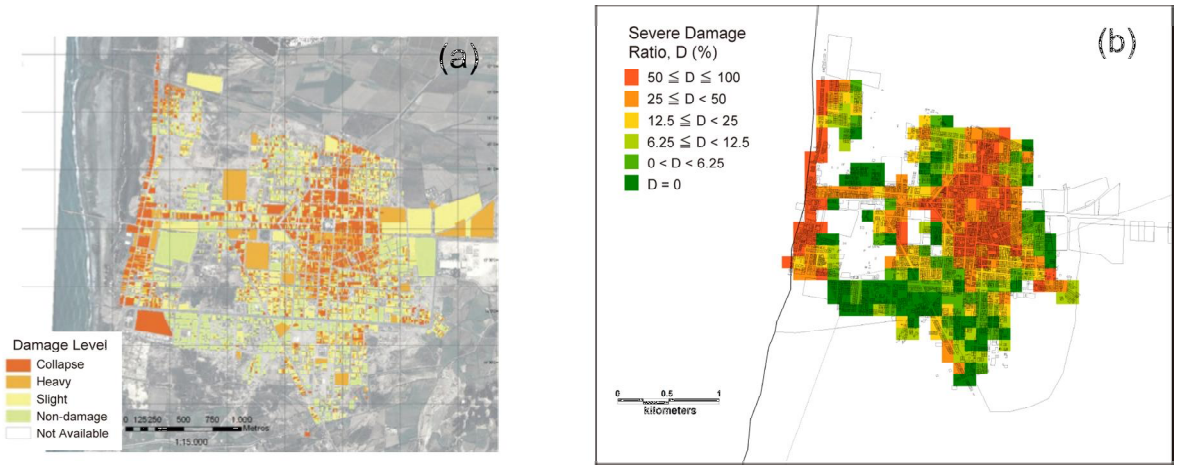

Figure 2: Building damage data in Pisco based on the field survey. (a) Damage level by lot (Estrada et al., 2008). (b) Distribution of the severe damage ratio.

ESTIMATION OF SEVERE DAMAGE RATIO BASED ON REGRESSION DISCRIMINANT FUNCTION

The influence of window size on the accuracy of damage discrimination

In previous studies (Matsuoka and Yamazaki, 2004; Nojima et al., 2006; Matsuoka and Yamazaki, 2010; Matsuoka and Nojima, 2010), a speckle reduction filter with a 21 × 21 pixel window was applied to SAR images and the differences and correlation coefficients were calculated from a 13 × 13 pixel window. Although these window sizes suited extraction of the damaged area from 30-m resolution SAR imagery of an area affected by the Kobe earthquake and field survey data in the Hanshin area (Matsuoka and Yamazaki, 2004), it was uncertain whether the window sizes would be the optimum for extraction of damage in a city in Peru, in which building types are different from those in the Hanshin area, with approximately 10-m resolution, which is the same with the resolution of PALSAR imagery. Accordingly, the change in the accuracy of damage discrimination was examined with varying a speckle reduction filter size and calculation window size for data sets of Pisco.

First, the influence of speckle reduction filters was examined. A Lee filter size that is variable from 3 × 3 to 51 × 51 pixels was applied to the pre- and post-event images and the differences and correlation coefficients were calculated based on equations (1) and (2). The images of the differences and the correlation coefficients were overlaid on the field survey data and 800 pixels were randomly extracted from areas corresponding to each of the six damage ranks shown in Table 1 (4,800 pixels in total) to create a training sample. For a quantitative evaluation of the severe damage ratio, regression discriminant analysis (Okuno et al., 1981), a method of multiple-group discriminant that uses the differences and the correlation coefficients of the six damage ranks, was applied. For calculation of the differences and the correlation coefficients, window sizes of 7 × 7, 13 × 13, and 21 × 21 pixels were examined. Figure 3 shows the correlation ratio of regression discriminant functions representing the ability to discriminate six damage ranks against the pixel dimension calculated from the size of a speckle reduction filter. In this figure, a larger correlation ratio means a better discriminant ability of damage ranks. The relationship between the pixel dimension and the correlation ratio is slightly complicated; as the size of the filter increases, the correlation ratio decreases but turns upward at around 15 × 15 pixels. However, the correlation ratio obtained when the filter size is increased to the largest one, 41×41 pixels, is almost the same as that obtained without any filter; therefore it was determined that no filter would be used in this study.

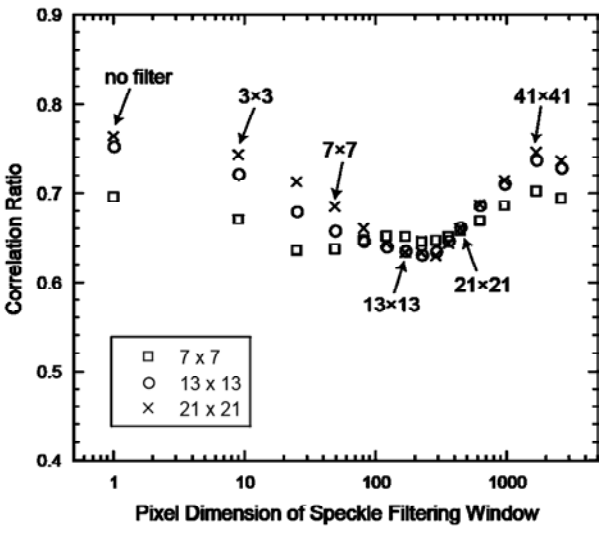

Figure 3: Relationship between the size of speckle reduction filters and the correlation ratio

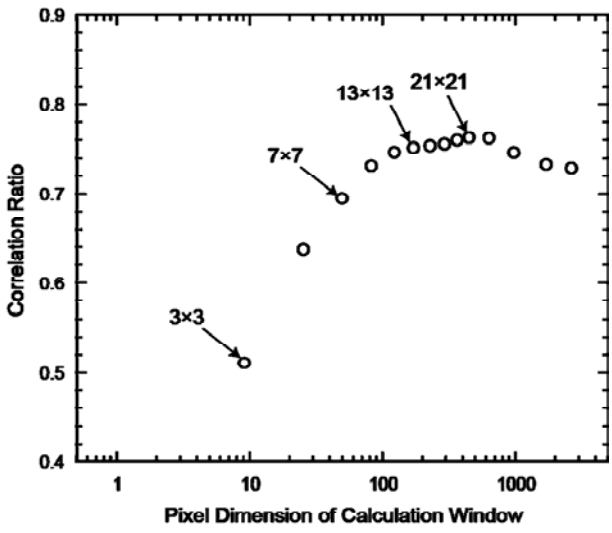

Figure 4: Relationship between the calculation window size and the correlation ratio

Next, the influence of window size on the accuracy of discrimination was examined. With varying window size, from 3 × 3 to 51 × 51 pixels, used for calculation of the differences and the correlation coefficients, the correlation ratio of regression discriminant functions was calculated. Figure 4 shows the correlation ratio against the

pixel dimension calculated from the window size. As the window size increased from 3 × 3, the correlation ratio increased and reached a limit at around 13 × 13 pixels. This tendency was also found for data sets in the Hanshin area before and after the Kobe earthquake (Matsuoka and Yamazaki, 2004). The reasons why the correlation ratio increases includes that damaged building groups spread to some extent and, in addition, backscattering of each damaged building has a spatial extent. It is interesting that although the pixel size of SAR images in the Hanshin area and Pisco are different, the window size at which the correlation ratio reached a limit was the same, around 13 × 13 pixels. Although this is considered to arise from complex factors such as the fact that different damage situations are involved, the detail remains a challenge to be addressed. It should be noted that although the correlation ratio reached a maximum in Figure 4 when 21 × 21 pixels were used, the value is almost the same as that of 13 × 13 pixels; the window size of 13 × 13 pixels, which was used in the previous study, will be used in this study.

Derivation of regression discriminant function and likelihood function

For calculation of difference d and correlation coefficient r, a window size of 13 × 13 pixels was adopted as an optimum window size for interpretation of damage in Pisco based on analysis of the data sets, and no speckle reduction filter was used. Figure 5 shows a scatter diagram by damage rank. A regression discriminant function was calculated from the two indices is shown in equation (3):

$$Z_{Rp} = -0.089\, d - 2.576\, r \qquad (3)$$

where Z_{Rp} represents the discriminant score derived from PALSAR imagery. While coefficients of d and r in the discriminant score Z_{Rj} derived from JERS-1/SAR imagery of the Kobe earthquake were −1.277 and −2.729, respectively (Matsuoka and Nojima, 2010), the coefficients derived here from PALSAR imagery of Pisco were −0.089 and −2.576. Coefficients of d and r indicate the degree of influence of d or r on the discriminant score. Comparison between the Hanshin area and Pisco demonstrated that the coefficients of r, the correlation coefficient, were almost the same in the two regions, but the coefficient of d, the difference in backscattering coefficients, of Pisco was small, or approximately zero, as compared with that of the Hanshin area. It can thus be said that the influence of d on discrimination of damage rank in Pisco is not so large.

Next, following similar procedures to those in the previous study (Nojima et al., 2006; Matsuoka and Nojima, 2010), a likelihood function for estimating the severe damage ratio from the discriminant score Z_{Rp} is formed. The likelihood function in this study means the probability of being in each damage rank when Z_{Rp} is given. Specifically, the frequency distribution of Z_{Rp} of 800 randomly extracted pixels from each damage rank is modeled as a normal distribution. Figure 6 shows normal distribution models (likelihood function). Table 2 shows the average values and standard deviations of Z_{Rp} for each damage rank. The higher the damage rank, the larger the discriminant score, Z_{Rp}. However, because the distribution curves of some damage ranks cross in regions with low discriminant scores, discrimination in areas with low damage ranks is impossible. Figure 7 shows normalized likelihood functions, in which the sum of the likelihood of all damage ranks in Figure 6 would become 1. For the regions where Z_{Rp} is −2.2 or under, a constant value obtained by extrapolating the value at Z_{Rp} = −2.2 is used in order to avoid a reversal of sequence of the severe damage ratio caused by the distribution curves crossing. The average values and standard deviations of the estimated severe damage ratio against the discriminant score Z_{Rp} can then be obtained from the median values of the damage rank in Table 1 and the distribution shown in Table 2 and Figure 7. Figure 8 shows curves of the average values and the average values ± standard deviations of the severe damage ratio estimated from Z_{Rp}. The severe damage ratio increases with increasing Z_{Rp}. Because the discriminant score was adjusted to make the constant term be zero, relative positions on the horizontal axis in Figure 8 are arbitrary. Taking this into account, the normalized likelihood function derived from the field survey data and PALSAR imagery of Pisco gives a high severe damage ratio (average value) in regions with low discriminant scores compared with that derived from the field survey data and JERS-1/SAR imagery of the Hanshin area (Matsuoka and Nojima, 2010) (shown in Figure 8 together). It also indicates that small changes in backscattering characteristics have a large influence on the estimation of the severe damage ratio. It could be influenced by the differences in building damage situations between Pisco and the Hanshin area.

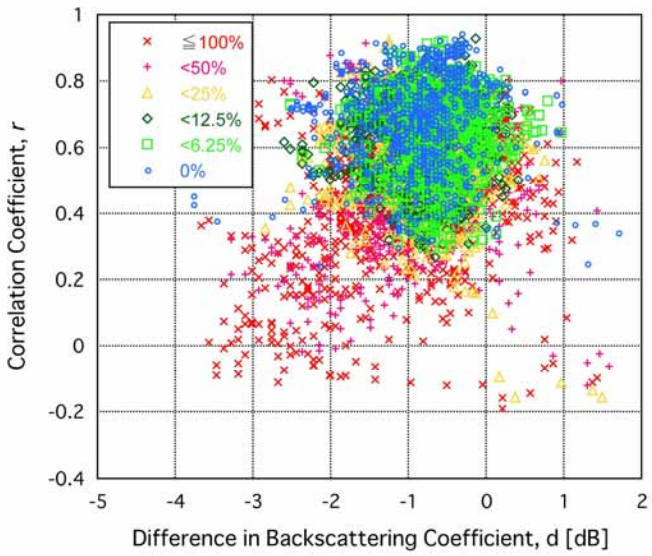

Figure 5: Relationship between the differences in backscattering coefficients and correlation coefficients for each damage rank

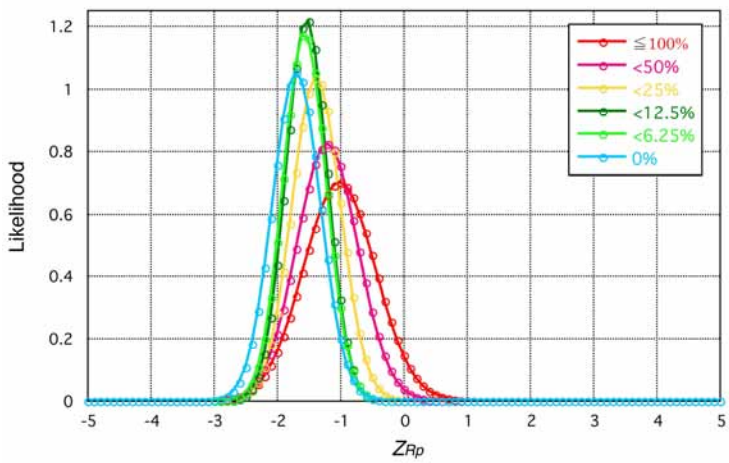

Figure 6: Normal distribution model of frequency distribution of the discriminant score Z_{Rp}

Table 2: Average values and standard deviations of likelihood function of data on PALSAR intensity imagery

Damage Rank	Average of Z_{Rp}	Standard Deviation
C1	-1.470	0.323
C2	-1.355	0.291
C3	-1.332	0.281
C4	-1.200	0.331
C5	-1.052	0.415
C6	-0.887	0.484

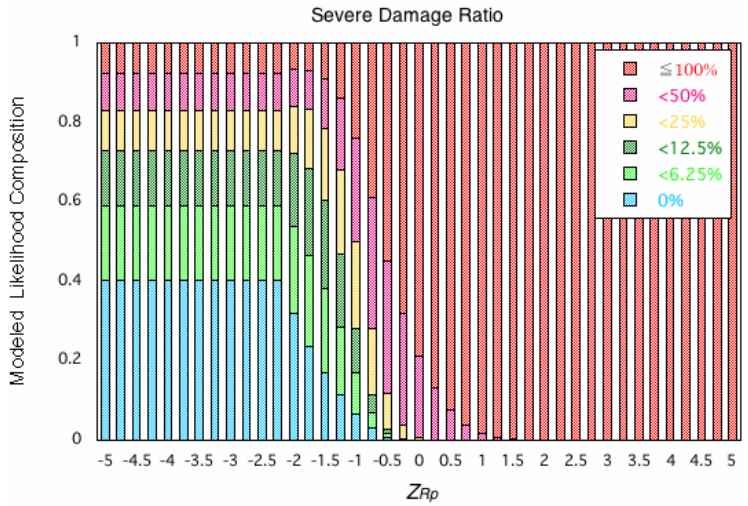

Figure 7: Normalized likelihood function of the discriminant score Z_{Rp}

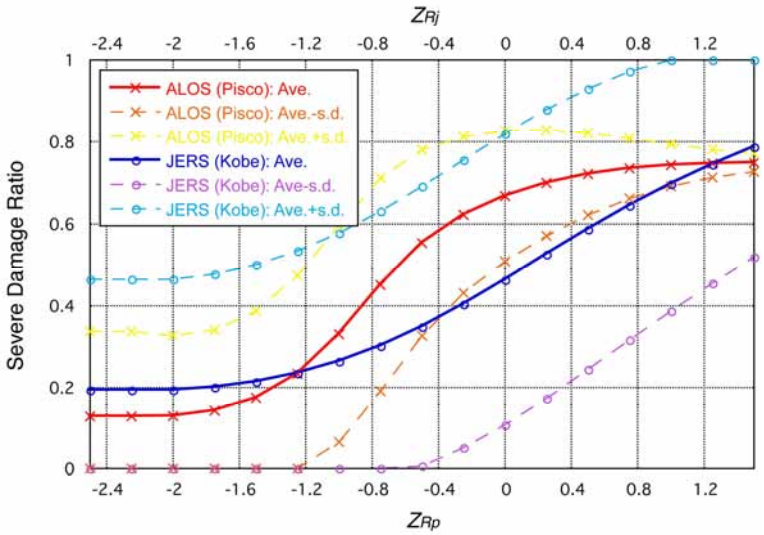

Figure 8: Relationship between the severe damage ratio (average values and standard deviations) and the discriminant scores of Pisco Z_{Rp} and Hanshin Z_{Rj}

Figure 9 shows the Z_{Rp} distribution obtained from pre- and post-earthquake PALSAR images and Figure 10 shows the severe damage ratio (average values) estimated from Z_{Rp}. Z_{Rp} values and the severe damage ratio are slightly large at the center of Pisco. It should be noted that the target area is restricted to urban areas where the cardinal effect can be expected; therefore, areas whose backscattering coefficients are small (−5 dB or under) in the pre-event images are masked. The distribution of severe damage ratio in Pisco city estimated based on PALSAR imagery is in good agreement with the field survey data. However, areas with high severe damage ratios are found in sections of farmland because they are not adequately masked owing to variations in backscattering characteristics caused by vegetation.

CONCLUSIONS

To develop a technology to quickly assess areas affected by earthquakes using imagery of L-band synthetic aperture radar (SAR) mounted on satellites, an estimation model of severe damage ratio of buildings, optimized for Peru, was created based on field survey data and PALSAR imagery of the city of Pisco struck by the 2007 Peru earthquake. Regression discriminant analysis was performed, in which the explanatory variables, namely

differences and correlation coefficients, were calculated from pre- and post-earthquake PALSAR images. The target groups included six damage ranks that were classified based on the severe damage ratio of buildings. Examination of an optimum window size for calculation of the differences and correlation coefficients resulted in the same parameter as that obtained from data from the 1995 Kobe earthquake. A regression discriminant function was derived that takes into consideration urban structures, building types, the damage situation in Peru, and pixel resolution of PALSAR imagery. Furthermore, normalized likelihood functions for the severe damage ratio were obtained from the discriminant score of the regression discriminant function. If an earthquake occurs in Peru in the future, the model proposed in this study can be used for damage assessment.

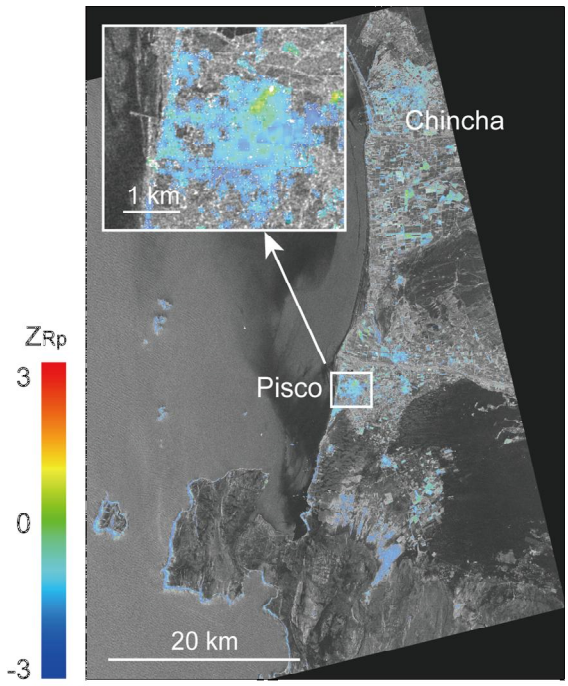

Figure 9: Discriminant score Z_{Rp} estimated from PALSAR imagery

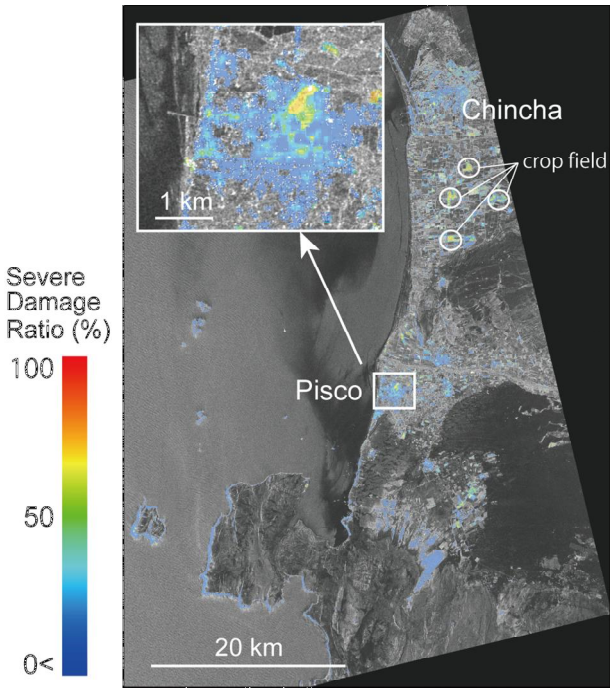

Figure 10: Severe damage ratio of buildings, estimated from normalized likelihood function (average values)

ACKNOWLEDGMENT:

The PALSAR data are the property of the Ministry of Economy, Trade and Industry (METI) and the Japan Aerospace Exploration Agency (JAXA) and processed with GEO Grid of the National Institute of Advanced Industrial Science and Technology (AIST). This study was supported in part by a Science and Technology Research Partnership for Sustainable Development (SATREPS) project, titled "Enhancement of Earthquake and Tsunami Disaster Mitigation Technology in Peru (Principal Investigator: Fumio Yamazaki)."

REFERENCES:

Arciniegas, G. A., Bijker, W., Kerle, N., Tolpekin, V. A., 2007. Coherence- and Amplitude-based Analysis of Seismogenic Damage in Bam, Iran, Using Envisat ASAR Data, Transactions on Geoscience and Remote Sensing, 45, pp.1571–1581.

Estrada, M., Zavala, C., Aguilar, Z., 2008. Damage Study of the Pisco, Peru Earthquake using GIS and Satellite Images, Proceedings of International Workshop for Safer Housing in Indonesia and Peru.

Ghosh, S., Huyck, C. K., Greene, M., Gill, S. P., Bevington, J., Svekla, W., DesRoches, R., Eguchi, R. T., 2011. Crowdsourcing for Rapid Damage Assessment: The Global Earth Observation Catastrophe Assessment Network (GEO-CAN), Earthquake Spectra, 27(S1), pp.S179-S198.

Grünthal, G., 1998. European Macroseismic Scale 1998 (EMS-98), European Seismological Commission.

International Charter Space and Major Disaster, 2012. http://www.disasterscharter.org, as of February 2012.

Ito, Y., Hosokawa, M., 2002. An Estimation Model of Damage Degree using Interferometric SAR data, IEEJ Transactions on Electronics, Information and Systems, 122-C(4), pp.617-623 (in Japanese with English abstract).

Lee, J. S., 1980. Digital Image Enhancement and Noise Filtering by Use of Local Statistics, IEEE Trans. Pattern Analysis and Machine Intelligence, 2(2), pp.165-168.

Matsuoka, M., Nojima, N., 2010. Building Damage Estimation by Integration of Seismic Intensity Information and Satellite L-band SAR Imagery, Remote Sensing, MDPI, 2(9), pp.2111-2126.

Matsuoka, M., Yamazaki, F., 2004. Use of Satellite SAR Intensity Imagery for Detecting Building Areas Damaged due to Earthquakes, Earthquake Spectra, 20(3), pp.975-994.

Matsuoka, M., Yamazaki, F., 2010. Comparative Analysis for Detecting Areas with Building Damage from Several Destructive Earthquakes Using Satellite Synthetic Aperture Radar Images, Journal of Applied Remote Sensing, SPIE, 4, 041867.

Midorikawa, S., Miura, H., 2010. Extraction of Landslide Areas due to the 2008 Iwate-Miyagi-Nairiku, Japan Earthquake from High-Resolution SAR Image, Journal of Japan Association for Earthquake Engineering, 10(3), pp.25-32 (in Japanese with English abstract).

Nojima, N., Matsuoka, M., Sugito, M., Ezaki, K., 2006. Quantitative Estimation of Building Damage Based on Data Integration of Seismic Intensities and Satellite SAR Imagery. Journal of JSCE, Division A, 62(4), pp.808-821 (in Japanese with English abstract).

Okuno, T., Kume, H., Haga, T., Yoshizawa, T., 1981. Multivariate Statistical Methods; Union of Japanese Scientists and Engineers, Tokyo, Japan, pp. 259-321 (in Japanese).